FtsW exhibits distinct processive movements driven by either septal cell wall synthesis or FtsZ treadmilling in *E. coli*

Xinxing Yang[1], Ryan McQuillen[1], Zhixin Lyu[1], Polly Phillips-Mason[2], Ana De La Cruz[1], Joshua W. McCausland[1], Hai Liang[3,5], Kristen E. DeMeester[3], Catherine L. Grimes[3,4], Piet de Boer[2*], Jie Xiao[1*]

[1]Department of Biophysics and Biophysical Chemistry, Johns Hopkins School of Medicine, Baltimore, Maryland, 21205, USA.

[2]Department of Molecular Biology & Microbiology, School of Medicine, Case Western Reserve University, Cleveland, Ohio 44106-4960, USA.

[3]Department of Chemistry and Biochemistry, University of Delaware, 134 Brown Lab, Newark, Delaware 19716, USA.

[4]Department of Biological Sciences, University of Delaware, Newark, Delaware 19716, USA.

[5]Current address: Dermatology Branch, National Institute of Arthritis and Musculoskeletal and Skin Diseases, NIH, Bethesda, MD 20892, USA

*Correspondence and requests for materials should be addressed to P.d.B. (email: pad5@case.edu) and J.X. (email: xiao@jhmi.edu)

Abstract

During bacterial cell division, synthesis of new septal peptidoglycan (sPG) is crucial for successful cytokinesis and cell pole morphogenesis. FtsW, a SEDS (Shape, Elongation, Division and Sporulation) family protein and an indispensable component of the cell division machinery in all walled bacterial species, was recently identified *in vitro* as a new monofunctional peptidoglycan glycosyltransferases (PGTase). FtsW and its cognate monofunctional transpeptidase (TPase) class b penicillin binding protein (PBP3 or FtsI in *E. coli*) may constitute the essential, bifunctional sPG synthase specific for new sPG synthesis. Despite its importance, the septal PGTase activity of FtsW has not been documented *in vivo*. How its activity is spatiotemporally regulated *in vivo* has also remained unknown. Here we investigated the septal PGTase activity and dynamics of FtsW in *E. coli* cells using a combination of single-molecule imaging and genetic manipulations. We showed that FtsW exhibited robust activity to incorporate an *N*-acetylmuramic acid analog at septa in the absence of other known PGTases, confirming FtsW as the essential septum-specific PGTase *in vivo*. Furthermore, we identified two populations of processively moving FtsW molecules at septa. A fast-moving population is driven by the treadmilling dynamics of FtsZ and independent of sPG synthesis. A slow-moving population is driven by active sPG synthesis and independent of FtsZ treadmilling dynamics. We further identified that FtsN, a potential sPG synthesis activator, plays an important role in promoting the slow-moving, sPG synthesis-dependent population. Our results support a two-track model, in which inactive sPG synthase molecules follow the fast treadmilling "Z-track" to be distributed along the septum; FtsN promotes their release from the "Z-track" to become active in sPG synthesis on the slow "sPG-track". This model integrates spatial information into the regulation of sPG synthesis activity and could serve as a mechanism for the spatiotemporal coordination of bacterial cell wall constriction.

To investigate the role of FtsW in sPG synthesis *in vivo*, we employed a cysteine-modification inactivation assay[1,2]. Based on the homology structure of RodA[3], we generated twelve *ftsW*^{C} alleles that

each encodes a unique cysteine residue on the periplasmic side of FtsW (Extended Data Fig. 1 and Supplementary Table 1). Amongst these, we identified FtsW^{I302C} as a promising candidate for *in vivo* inactivation with the cysteine-reactive reagent MTSES (2-sulfonatoethyl methanethiosulfonate)[4]. Cells expressing FtsW^{I302C} from the native chromosomal *ftsW* locus grew with a wild-type (WT)-like doubling time and cell morphology in the absence of MTSES but grew into long chains and stopped dividing when treated with MTSES (Extended Data Fig. 2, Supplementary Movie 1, 2). WT parental BW25113 cells treated with MTSES did not show any appreciable cell division defect (Extended Data Fig. 2), indicating that MTSES specifically inhibited the essential function of FtsW^{I302C}. The homology structure of FtsW indicates that I302 resides in the periplasmic loop 4 between transmembrane helices 7 and 8, likely near critical residues of the PGTase activity of SEDS proteins[3,5].

To probe the contribution of FtsW to sPG synthesis *in vivo*, we labeled new cell wall peptidoglycan (PG) synthesis using an alkyne-modified N-acetylmuramic acid (alkyne-NAM). Unlike fluorescent D-amino acid (FDAA) labels, which are incorporated into the peptide stem of *E. coli* PG through periplasmic exchange reactions[6], alkyne-NAM enters the endogenous cytoplasmic PG biosynthetic pathway and incorporates into newly linked glycan chains[7] composed of alternating units of NAM and *N*-acetylglucosamine (NAG). Subsequent labeling of the alkyne using a fluorophore-conjugated azide by copper catalyzed azide-alkyne cycloaddition (CuAAC) also known as "CLICK" chemistry allows for visualization and quantification of newly polymerized glycan strands[8].

In WT cells treated with or without MTSES, we observed robust NAM labeling (2 mg/ml, 30 min, Fig. 1a**,** Methods) at septa. In *ftsW*^{I302C} cells treated with MTSES (1 mM, 30 min), we observed a significant reduction in the percentage of cells showing septal labeling above the background level (from 34 ± 4% to 22 ± 4%, μ ± S.E.M., N > 300 cells, three independent repeats, Fig. 1b, orange bars, Supplementary Table 3). Furthermore, in this septal-labeled population of MTSES-treated *ftsW*^{I302C} cells, the median fluorescence intensity dropped to 70 ± 4% compared to that in untreated cells (Extended Data Fig. 3, Supplementary Table 3). Thus, inhibition of FtsW^{I302C} activity by MTSES caused a total reduction

in septal NAM labeling of ~ 55% (100% – 22% / 34% × 70%, Fig. 1c, orange bar), consistent with a major role of FtsW in septal glycan chain polymerization. The fact that significant NAM incorporation still occurred at septa of MTSES-treated *ftsW*^{I302C} cells is consistent with the previous report showing that FtsW is not an essential lipid II flippase acting upstream of sPG synthesis[9] and that other PGTases contribute to septal morphogenesis as well[10]. The inability of MTSES-treated *ftsW*^{I302C} cells to complete cell division, even when other PGTases are still active, highlights the essential role of FtsW in successful cell wall constriction.

To further investigate the relative contributions to sPG polymerization by FtsW and other relevant PGTases in *E. coli*, we introduced the chromosomal f*tsW*^{I302C} allele into a *Δ3 ponB*^{S247C} strain background[1] to create a *Δ3 ponB*^{S247C} *ftsW*^{I302C} strain. The *Δ3 ponB*^{S247C} strain lacks the genes for PBP1A, PBP1C and MtgA, and expresses a variant (S247C) of PBP1B (PBP1B^{S247C}, encoded by *ponB*^{S247C}) that, like FtsW^{I302C}, can be inactivated by exposure to MTSES. Untreated *Δ3 ponB*^{S247C} cells exhibited a similar percentage of labeled septa as WT cells (32 ± 1%, μ ± S.E.M., N > 300 cells, three independent repeats, Fig. 1b, blue bar, Supplementary Table 3), indicating that PBP1A, PBP1C and MtgA together contribute minimally to the essential sPG polymerization activity under our experimental condition. When the PGTase activity of PBP1B^{S247C} in *Δ3 ponB*^{S247C} cells was inhibited by MTSES, the percentage of labeled septa dropped to 14 ± 3 % with the median intensity reduced to 65 ± 12 % of the WT MTSES-treated level (Fig. 1b, blue bar, Supplementary Table 3), corresponding to a total loss of septal labeling of ~ 72 % (100% – 14% / 32% × 65% Fig. 1c, blue bar). Simultaneous inactivation of PBP1B and FtsW by MTSES in *Δ3 ponB*^{S247C} *ftsW*^{I302C} cells, however, led to a background level of septal NAM labeling indistinguishable from that when the essential Lipid II flippase MurJ[9] was inhibited (Fig. 1b, c, compare purple and gray bars, Supplementary Table 3). These results strongly support that FtsW and PBP1B are the two major septal PGTases, and that FtsW is the only essential septum-specific monofunctional PGTase.

Previously, we and others showed that FtsZ's treadmilling dynamics drive the processive movement of FtsW's cognate TPase (FtsI in *E. coli* and PBP2B in *B. subtilis*) at septa[11,12]. Such FtsZ-dependent dynamics were proposed to direct the spatial distribution of sPG synthesis complexes and play an important role in septum morphogenesis[11,12]. Because a large body of biochemical and genetic studies indicates that FtsW associates with FtsI to form a bifunctional sPG synthase complex[13-15], we investigated whether FtsW exhibited similar processive movement at septa using single molecule tracking (SMT).

We constructed a C-terminal fusion of FtsW with the red fluorescent protein TagRFP-t (Supplementary Table 1) and will refer to the fusion protein as FtsW-RFP for simplicity. We verified that upon replacement of chromosomal *ftsW* with the *ftsW-rfp* allele (strain JXY422), FtsW-RFP localizes correctly to midcell and supports normal cell division under our experimental conditions (Extended data Fig. 2). To enable single-molecule detection, we expressed FtsW-RFP ectopically at a low level (plasmid pXY349) in the presence of WT FtsW in BW25113 cells. We tracked the dynamics of single FtsW-RFP molecules at midcell with a frame rate of 2 Hz using wide-field fluorescence microscopy. This slow frame rate allowed us to focus on septum-localized FtsW-RFP molecules by effectively filtering out fast, randomly diffusing molecules along the cylindrical part of the cell body. Using a custom-developed unwrapping algorithm (Extended Data Fig. 4, Methods), we decomposed two-dimensional (2D) trajectories of individual FtsW-RFP molecules obtained from the curved cell surfaces at midcell to one-dimensional (1D) trajectories along the circumference and long axis of the cell respectively (Fig. 2, Extended Data Fig. 4, Methods).

We found that single FtsW-RFP molecules displayed heterogenous dynamics at midcell. Some FtsW-RFP molecules were relatively stationary and confined to small regions (Fig. 2a-c, Supplementary Movie 3), some moved processively along the cell circumference (Fig. 2d-f, Supplementary Movie 4), and many dynamically transitioned between these states (Fig. 2g-i, Extended Data Fig. 5, Supplementary Movie 5-9). To quantitatively identify different movements and corresponding speeds, we split each trajectory into multiple segments and identified each as stationary or directional movement based on the

corresponding displacement along the midcell circumference (Methods). Segments of directional movement were fit to a straight line to extract the directional moving speed *v* (Fig. 2e, h, Extended Data Fig. 5, Methods). We quantified that, on average, a FtsW-RFP molecule was stationary for about half the time (51% ± 2%, μ ± S.E.M, D = 0.0019 $\mu m^2/s$, from 695 trajectories), and spent the other half time moving processively along the midcell circumference (Supplementary Table 4).

Notably, the speeds of all directionally moving FtsW-RFP molecules showed a much wider distribution (Fig. 2j, second panel and k; μ ± s.d. at 23 ± 30 nm/s, n = 320 segments) and displayed an additional slow-moving peak (Fig. 2j, second panel, green curve) when compared to the distribution of FtsZ's treadmilling speed[11] (Fig. 2j, top panel, blue curve). The corresponding cumulative probability density function (CDF) of FtsW-RFP's speed distribution was best fit by the sum of two populations, one fast and one slow, instead of one single fast population as that for the FtsZ treadmilling speed distribution (Fig. 2l, Extended Data Fig. 6a). The fast-moving population (~ 64 ± 16 %, μ ± S.E.M., n = 320 segments) of FtsW-RFP displayed a mean speed of 30 ± 3 nm/s, (μ ± S.E.M., Fig. 2j, second panel, red curve, Supplementary Table 4), similar to the average FtsZ treadmilling speed we previously measured[11] (28± 1 nm/s, μ ± S.E.M.). The slow-moving population (~ 36 ± 16 %, μ ± S.E.M.) of FtsW-RFP molecules had an average speed of ~ 8 nm/s (8 ± 1 nm/s, Fig. 2j, top, green curve, Supplementary Table 4). The presence of, and transition between, the two different types of directional movements could also be directly observed in many individual FtsW-RFP trajectories (Fig. 2h, Extended Data Fig. 5).

To investigate how the two directionally moving populations respond to FtsZ's treadmilling dynamics, we performed SMT of FtsW-RFP in five strains with mutations that affect FtsZ GTPase activity (*ftsZ*^{E238A}, *ftsZ*^{E250A}, *ftsZ*^{D269A}, *ftsZ*^{G105S} and *ftsZ*^{D158A}). We previously showed that in these strains the average directional moving speed of FtsI responds linearly to reduced FtsZ treadmilling speed with decreasing GTPase activity[11]. Here we found that in these FtsZ GTPase mutant backgrounds the average speed of all moving FtsW-RFP molecules correlated linearly with FtsZ's treadmilling speed in a nearly

identical manner as what we previously observed for FtsI (Fig. 2k), suggesting that FtsW moves together with FtsI in a sPG synthase complex as expected[13-15].

Most interestingly, close inspection and CDF analysis of the two moving populations of FtsW-RFP in FtsZ GTPase mutants (Fig. 2j, l) revealed that the reduction of the average speed of all moving FtsW-RFP molecules was primarily caused by reduced speeds of the fast-moving populations, whereas the slow-moving populations maintained a relatively constant speed (Fig. 2m, Extended Data Fig. 6, Supplementary Table 4). The differential responses of the two moving FtsW populations to FtsZ treadmilling dynamics suggest that the fast-moving population is driven by FtsZ treadmilling dynamics, while the slow-moving population is not. Note that a recent study showed that in *S. pneumoniae* the FtsW-PBP2x pair only exhibited one single directional moving population that is FtsZ-independent[16].

Additionally, we observed that on average FtsW-RFP spent more time in the stationary state as FtsZ GTPase activity decreased (Extended Data Fig. 7a, Supplementary Table 4). Speed distributions immediately before and after stationary interludes also shifted significantly to high speeds (Extended Data Fig. 7b). Given that the total sPG synthesis activity is not affected in these FtsZ GTPase mutants[11,17], and that FtsW or FtsI could track the shrinking end of a treadmilling FtsZ filament through a Brownian Rachet mechanism (our unpublished data), these observations indicate that stationary FtsW-RFP molecules are likely the ones immobilized in the middle of FtsZ filaments before it starts to track or after it dissociates from a treadmilling FtsZ filament. The increased time FtsW-RFP molecules spent in the stationary state in these FtsZ GTPase mutants likely reflects the increased time it takes for the end of a treadmilling FtsZ polymer with a reduced speed to come across a stationary FtsW-RFP molecule to mobilize it under these experimental conditions.

In *E. coli*, the cell wall constriction rate is not limited by FtsZ treadmilling speed but dependent on sPG synthesis activity[11,17]. Therefore, it is unlikely that the FtsZ-dependent, fast-moving FtsW molecules are active in sPG synthesis. Rather, the FtsZ-independent population could represent

164 catalytically active molecules with their slow speed reflecting processive sPG synthesis. To examine this
165 possibility, we tracked FtsW-RFP molecules under conditions of altered sPG synthesis activity.

166 We first tracked the movement of FtsW^{I302C}-RFP molecules in the BW25113 *ftsW*^{I302C}
167 background (JXY559/pAD004) in the absence and presence of MTSES. In the absence of MTSES, we
168 again observed two directionally moving populations of FtsW^{I302C}-RFP, one fast at 37 ± 9 nm/s and one
169 slow at 10 ± 1 nm/s (average speed at 22 ± 2 nm/s, μ ± s.e.m., N = 169 segments, Fig. 3a, b, black,
170 Supplementary Table 5). In the presence of MTSES, the slow-moving population of FtsW^{I302C}-RFP was
171 significantly depleted, as indicated by the right-shifted (higher speed) CDF curve, which can be well fit
172 by a single moving population with an average speed of 26 ± 2 nm/s (μ ± s.e.m., N = 272 segments, Fig.
173 3a, b, lime, Extended Data Fig. 8, Supplementary Table 5). Since MTSES specifically blocks FtsW^{I302C}-
174 dependent sPG synthesis (Fig. 1), these results support the hypothesis that the slow-moving FtsW-RFP
175 molecules represent the catalytically active form of FtsW.

176 To further confirm the correlation between sPG synthesis activity and the slow-moving
177 population of FtsW-RFP, we used cells with a superfission (SF) allele of *ftsW* (*ftsW*^{E289G}) that confers a
178 short-cell phenotype and alleviates the need for FtsN, an otherwise essential positive regulator of sPG
179 synthesis (Extended Data Fig. 9). SMT of FtsW^{E289G}-RFP in *ftsW*^{E289G} cells again revealed one fast- and
180 one slow-moving population (Fig 3a, dark green histogram), and the corresponding CDF curve shifted
181 significantly to the left (lower speeds) compared to that of FtsW-RFP in the parental WT TB28
182 background (Fig. 3a, gray histogram, and Fig. 3b, gray curve). Accordingly, the average speed of all
183 directional moving FtsW^{E289G}-RFP molecules in *ftsW*^{E289G} cells was significantly lower than that of FtsW-
184 RFP in WT cells (14 ± 1 vs 18 ± 2 nm/s, Supplemental Table 5). These results are consistent with the
185 hypothesis that the slow-moving population of FtsW is coupled to sPG synthesis activity.

186 Next, as FtsW and FtsI likely form a bifunctional sPG synthase complex and move together as we
187 showed above, inhibiting the crosslinking activity of FtsI might stall the FtsWI complex and reduce the

slow-moving, sPG synthesis-dependent population of FtsW. To examine this possibility, we specifically inhibited the TPase activity of FtsI using aztreonam (50 μg/ml, 30 min). We found that the distribution of directional moving speed of FtsW-RFP (Fig. 3c, purple) and the corresponding CDF curve (Fig. 3d, purple) shifted significantly to the right (faster speed) and was best fit by a single population with an average speed of 26 ± 2 nm/s (μ ± s.e.m., N = 238, Extended Data Fig. 8, Supplemental Table 5), similar to that in the FtsW^{I302C}-inhibited condition (Fig. 3a, b) and the treadmilling speed of FtsZ (Fig. 1l).

In contrast to what was observed in the FtsI-inhibited condition, we observed the opposite trend in the movement of FtsW-RFP in cells expressing a superfission variant of FtsI (FtsI^{S167I}). FtsI^{S167I} is similar to FtsW^{E289G} in alleviating the essentiality of FtsN but does so only partially (Extended Data Fig. 9). In *ftsI*^{S167I} cells, a major population of FtsW-RFP (72% ± 7%, N = 254 segments) moved at 6.0 ± 0.2 nm/s and a minor population moved at 19 ± 7 nm/s (Fig. 3c, d, red Supplementary Table 5). The resulting CDF curve also shifted significantly to the left (lower speed, Fig. 3d, red) compared to that of the WT parental strain (Fig. 3d, gray). These results are again consistent with the hypothesis that the slow-moving population is driven by sPG synthesis activity.

In *E. coli* under balanced growth, the cellular level of PG synthesis precursors limits cell growth and cell wall constriction rates[18,19]. Therefore, we reasoned that the slow-moving population of FtsW could also be modulated by the level of available PG precursors. To examine this possibility, we increased the PG precursor level by growing cells in a rich defined medium (EZRDM), which we previously showed to increase the cell wall constriction rate two-fold compared that in minimal M9 medium[17]. We found that the slow-moving population (11.0 ± 0.3 nm/s, μ ± s.e.m., N = 894 segments, Fig. 3e, f, yellow) increased from 36% ± 16 % in M9 to 52% ± 4 % in EZRDM, and the remaining fast-moving population in EZRDM displayed similar speed (29 ± 3 nm/s, μ ± s.e.m, , Fig. 3e, f, yellow, Supplemental Table 5) as in M9. In contrast, when cells were treated with Fosfomycin to inactivate MurA, the first essential enzyme towards synthesis of uridine diphosphate *N*-acetyl muramic acid(UDP-NAM) and Lipid II[20], the slow-moving (8 – 10 nm/s) population of FtsW-RFP molecules was drastically

diminished, while the population moving at the speed of FtsZ treadmilling (average speed at 25 ± 10 nm/s, N = 138 segments) persisted (Fig. 3e, f, orange, Extended Data Fig. 8, Supplementary Table 5). Additionally, we observed a population of FtsW-RFP molecules that moved even faster (average speed at 63 ± 14 nm/s, N = 138 segments, Supplementary Table 5). Why the latter population appeared is unclear, but it is conceivable that Fosfomycin-induced loss of overall cell wall integrity increases the number of very fast moving diffusive FtsW-RFP molecules that can be misinterpreted by the SMT algorithm as moving directionally.

In all the experiments described above, the slow-moving population of FtsW-RFP became depleted when sPG synthesis activity was reduced or abolished, but the population rather increased when sPG synthesis activity was enhanced. Additionally, the fraction of time a FtsW-RFP molecule spent in the stationary state correlated inversely with sPG synthesis activity: high sPG synthesis activity correlated with less time spent in stationary state and low sPG synthesis activity correlated with more time in stationary state (Fig. 3g, Supplemental Table 5),

Our results so far demonstrated that two directionally moving populations of FtsW exist *in vivo*. The fast-moving population is most likely driven by FtsZ treadmilling dynamics but inactive in sPG synthesis, whereas the slow-moving population is most likely active and driven by sPG synthesis. The presence of active and inactive FtsW populations brought up an interesting question: what determines the partitioning of the two populations? Previous studies in *E. coli* have shown that when FtsW and FtsI are first recruited to the division site by a complex of the FtsB, FtsL and FtsQ proteins (FtsBLQ), they are kept in an inactive state by the complex and cannot initiate sPG synthesis until FtsN, the last essential division protein to accumulate at the site, relieves the inhibitory effect of FtsQLB[21,22]. Therefore, FtsN may play an important role in triggering the transition of FtsW from the fast-moving (FtsZ-dependent) to slow-moving (sPG synthesis-dependent) state.

To test this hypothesis, we used an FtsN-depletion strain (EC1908)[23] wherein chromosomal *ftsN* is controlled by the *araBAD* regulatory region, and which grows and divides normally in the presence of

0.2% of arabinose (Extended Data Fig. 11, Supplementary Table 1). After overnight growth (~15 hours) in M9 medium without arabinose, the average cellular FtsN level was depleted to ~ 44% of that in WT type cells (Extended Data Fig. 11) and many cells grew into long filaments with shallow constrictions (Fig. 4a). We then tracked FtsW-RFP molecules at shallow constriction sites in these filamentous cells. Similar to the trend we observed above, there was a significant increase in the fraction of time FtsW-RFP stayed stationary (80 ± 2%) compared to WT cells (51 ± 2%, Supplementary Table 5). Most importantly, the slow-moving population of FtsW-RFP was drastically eliminated, and the remaining moving FtsW-RFP molecules moved at an average speed similar to FtsZ treadmilling (Fig. 4b, c, blue, Supplementary Table 5).

Next, to assess the effects of FtsN on FtsW dynamics under conditions were FtsN is no longer essential, we tracked the movements of FtsW-RFP in a *ftsB*^{E56A} superfission strain (BL167) that still produces FtsN, and also in strain BL173 (*ftsB*^{E56} Δ*ftsN*) that lacks FtsN completely. The *ftsB*^{E56A} superfission allele causes cells to initiate sPG synthesis earlier in the division cycle than normal, leading to a small-cell phenotype[21]. While it also allows cells to grow and divide in the complete absence of FtsN, *ftsB*^{E56A}*ΔftsN* cells divide less efficiently than wt and are modestly elongated[21] (Supplementary Table 6). In *ftsB*^{E56A} cells, we observed a significantly increased slow-moving population of FtsW (Fig. 4b, orange); the fast-moving, FtsZ-dependent population of FtsW-RFP was essentially abolished, and nearly all (90 ± 1%) directional moving FtsW-RFP molecules moved at an average speed of ~ 10 nm/s (10 ± 1 nm, Fig. 4b, c, orange, Supplementary Table 5). Most interestingly and as we expected, in *ftsB*^{E56A}*ΔftsN* cells where FtsN is absent, the slow-moving population of FtsW-RFP was reduced while the fast-moving population recovered to approximately the same level as that in WT cells (Fig 4b,c, yellow, Supplementary Table 5). These results demonstrated that even though FtsN is no longer essential in the superfission *ftsB*^{E56A} background, it still contributes to the transitioning of FtsW from the fast-moving, FtsZ-dependent state to the slow-moving, sPG synthesis-dependent mode.

To summarize our observations in this work, in Fig. 5a we plotted and sorted form low to high the average speeds of all directionally moving FtsW-RFP molecules under conditions where sPG synthesis activity was altered. We observed a clear anti-correlation of the average directional moving speed of FtsW with expected sPG synthesis activity qualitatively: FtsW moves fast when sPG synthesis activity was reduced or abolished, and slowly when sPG synthesis activity was elevated (Fig. 5a), due to the partitioning of FtsW between the fast-moving, FtsZ-dependent population and the slow-moving, sPG-dependent population (Extended Data Fig. 12a). Additionally, the fraction of time FtsW spent in the stationary state anti-correlated with sPG synthesis activity: FtsW spent more time in the stationary state when sPG synthesis was reduced or abolished, and less time when sPG synthesis activity was elevated (Extended Data Fig. 12b). Notably, a recent study showed that the directional movement of PBP2 (the counterpart of FtsI in cell wall elongation machinery in *E. coli*) also depends on the cell wall synthesis activity but not the cytoskeleton protein MreB[24].

Taken together, our data support a two-track model (Fig. 5b), in which FtsW, and most likely FtsI and possibly other sPG remodeling enzymes and regulators as well, occupy at least two 'tracks' within the septum: a fast 'Z-track' representing inactive molecules associated with treadmilling FtsZ polymers, and a slower 'sPG-track' representing active molecules that exited the Z-track to produce sPG processively. Some of these molecules could also remain stationary when they are not mobilized by either one of the tracks. FtsN promotes the release of inactive sPG synthase from treadmilling FtsZ polymers to pursue the sPG-track for active synthesis. In this scenario, FtsWI may associate with the suppression complex FtsBLQ on the Z-track in an inactive state, and switch to associate with the activator FtsN on the sPG track to become active. Further investigations to examine the dynamics of the FtsQLB and FtsN will help elucidate these possibilities. This two-track model integrates spatial information into the regulation of sPG synthesis activity and could serve as a novel mechanism for the spatiotemporal coordination of bacterial cell wall constriction.

Acknowledgements

The authors thank lab members in the Xiao and de Boer labs for helpful discussions and technical assistance, Dr. G. Hauk for sharing plasmids and the CRISPR-Cas9/λ-red recombineering cloning method, Dr. D. S. Weiss for the EC1908 strain, pDSW406 plasmid, anti-FtsN serum, and helpful suggestions on FtsW immunoblot, Dr. T. Berhardt for HC532 strain, Dr. E. Goley for the help on cell growth measurement. Dr. R. Tsien for the TagRFP-T construct. This work was supported by NIH R01 GM57059 (to P.d.B), NIH R01 GM086447 (to J.X.), GM125656 (subcontract to J.X.), NSF EAGER Award MCB-1019000 (to J.X.), and a Hamilton Smith Innovative Research Award (to J.X.)

Reference:

1. Cho, H. *et al.* Bacterial cell wall biogenesis is mediated by SEDS and PBP polymerase families functioning semi-autonomously. *Nat Microbiol* **1,** 16172 (2016).

2. Butler, E. K., Davis, R. M., Bari, V., Nicholson, P. A. & Ruiz, N. Structure-function analysis of MurJ reveals a solvent-exposed cavity containing residues essential for peptidoglycan biogenesis in Escherichia coli. *J Bacteriol* **195,** 4639–4649 (2013).

3. Sjodt, M. *et al.* Structure of the peptidoglycan polymerase RodA resolved by evolutionary coupling analysis. *Nature* **556,** 118–121 (2018).

4. Karlin, A. & Akabas, M. H. Substituted-cysteine accessibility method. *Meth Enzymol* **293,** 123–145 (1998).

5. Meeske, A. J. *et al.* SEDS proteins are a widespread family of bacterial cell wall polymerases. *Nature* **537,** 634–638 (2016).

6. Kuru, E. *et al.* In Situ probing of newly synthesized peptidoglycan in live bacteria with fluorescent D-amino acids. *Angew Chem Int Ed Engl* **51,** 12519–12523 (2012).

7. Liang, H. *et al.* Metabolic labelling of the carbohydrate core in bacterial peptidoglycan and its applications. *Nat Commun* **8,** 15015 (2017).

8. Kolb, H. C., Finn, M. G. & Sharpless, K. B. Click Chemistry: Diverse Chemical Function from a Few Good Reactions. *Angew Chem Int Ed Engl* **40,** 2004–2021 (2001).

9. Sham, L.-T. *et al.* MurJ is the flippase of lipid-linked precursors for peptidoglycan biogenesis. *Science* **345,** 220–222 (2014).

10. Egan, A. J. F. & Vollmer, W. The physiology of bacterial cell division. *Ann N Y Acad Sci* **1277,** 8–28 (2012).

11. Yang, X. *et al.* GTPase activity-coupled treadmilling of the bacterial tubulin FtsZ organizes septal cell wall synthesis. *Science* **355,** 744–747 (2017).

12. Bisson-Filho, A. W. *et al.* Treadmilling by FtsZ filaments drives peptidoglycan synthesis and bacterial cell division. *Science* **355,** 739–743 (2017).

13. Di Lallo, G., Fagioli, M., Barionovi, D., Ghelardini, P. & Paolozzi, L. Use of a two-hybrid assay to study the assembly of a complex multicomponent protein machinery: bacterial septosome differentiation. *Microbiology (Reading, Engl)* **149,** 3353–3359 (2003).

14. Fraipont, C. *et al.* The integral membrane FtsW protein and peptidoglycan synthase PBP3 form a subcomplex in Escherichia coli. *Microbiology (Reading, Engl)* **157,** 251–259 (2010).

15. Karimova, G., Dautin, N. & Ladant, D. Interaction network among Escherichia coli membrane proteins involved in cell division as revealed by bacterial two-hybrid analysis. *J Bacteriol* **187,** 2233–2243 (2005).

16. Perez, A. J. *et al.* Movement dynamics of divisome proteins and PBP2x:FtsW in cells of Streptococcus pneumoniae. *Proc Natl Acad Sci USA* **116,** 3211–3220 (2019).

17. Coltharp, C., Buss, J., Plumer, T. M. & Xiao, J. Defining the rate-limiting processes of bacterial cytokinesis. *Proc Natl Acad Sci USA* **113,** E1044–53 (2016).

18. Lee, T. K. *et al.* A dynamically assembled cell wall synthesis machinery buffers cell growth. *Proc Natl Acad Sci USA* **111,** 4554–4559 (2014).

19. Rojas, E., Theriot, J. A. & Huang, K. C. Response of Escherichia coli growth rate to osmotic shock. *Proc Natl Acad Sci USA* **111,** 7807–7812 (2014).

20. Kahan, F. M., Kahan, J. S., Cassidy, P. J. & Kropp, H. The mechanism of action of fosfomycin (phosphonomycin). *Ann N Y Acad Sci* **235,** 364–386 (1974).

21. Liu, B., Persons, L., Lee, L. & de Boer, P. A. J. Roles for both FtsA and the FtsBLQ subcomplex in FtsN-stimulated cell constriction in Escherichia coli. *Mol Microbiol* **95,** 945–970 (2015).

22. Tsang, M. J., & Bernhardt, T. G. A role for the F ts QLB complex in cytokinetic ring activation revealed by an fts L allele that accelerates division. *Mol Microbiol* **95**, 925-944 (2015).

23. Tarry, M. *et al.* The Escherichia coli cell division protein and model Tat substrate SufI (FtsP) localizes to the septal ring and has a multicopper oxidase-like structure. *J Mol Biol* **386,** 504–519 (2008).

24. Wollrab, E., Özbaykal, G., Vigouroux, A. & Cordier, B. Transpeptidase PBP2 governs initial localization and activity of major cell-wall synthesis machinery in Escherichia coli. *BioRxiv* 716407 (2019).

Figure Legends

Figure 1. **FtsW is the only essential septum-specific monofunctional PGTase**. **a**. Representative images of *E. coli* cells of different strain backgrounds labeled with AF647-conjugated NAM in the absence or presence of MTSES. The contrast of each image is adjusted to allow optimized visualization of septal labeling especially for the *Δ3 ponB*^{S247C} *ftsW*^{I302C} and *murJ*^{A29C} + MTSES conditions. The absolute intensity is summarized in Supplementary Table 3. Scale bar: 1 μm. **b**. Mean percentage of cells with septal NAM labeling above background level in the absence or presence of MTSES. **c**. Mean percentage of total loss in septal NAM intensity of the five strains due to MTSES. Error bars: S.E.M. of three experimental repeats (dots). Strains used were BW25113 (*wt*), JXY559 (*ftsW*^{I302C}), HC532 (*Δ3 ponB*^{S247C}), JXY564 (*Δ3 ponB*^{S247C} *ftsW*^{I302C}), and JXY589 (*murJ*^{A29C}), all carrying plasmid pBBR1-KU.

Figure 2. **FtsW exhibits two processively moving populations that are differentially dependent on FtsZ's treadmilling dynamics**. **a, d and g:** Representative maximum fluorescence intensity projection images with superimposed single molecule trajectories (time-colored from blue to red) of two stationary FtsW-RFP molecules (**a**), one processively moving FtsW-RFP molecule (**d**), and one moving FtsW-RFP molecule that transitioned between different directions and speeds (**g**) in BW25113/ pXY349 cells (outlined in yellow). The corresponding kymographs are shown on the right. **b, e** and **h:** Unwrapped one-dimensional (1d) positions of the corresponding FtsW-RFP molecule along the circumference (red) and long axis (gray) of the cell. Positions along the circumference were fit with one or multiple straight lines to measure directional moving speeds (black). Positions along the long axis of the cell were used to confirm that the molecule remained at midcell. **c, f** and **i**: 1d MSD (mean squared displacement) of the corresponding FtsW-RFP molecule along the circumference (red) and long axis (gray) of the cell. FtsW-RFP molecule showed highly confined sub-diffusive motions in **c** and directional movement with average speeds of 8.4 nm/s and 13.9 nm/s in **f** and **i** respectively. **j**. Speed distribution (bars) of all processively moving FtsW-RFP molecules in FtsZ WT and GTPase mutants. The treadmilling speed distribution of

FtsZ adapted from [11] (blue) and the decomposed fast-moving (red) and slow-moving (green) populations of FtsW-RFP in WT cells were shown for comparison. The dashed green and red lines mark the speeds at 8 nm/s and 29 nm/s respectively for guide of eyes. **k**. Average speeds of all moving FtsW-RFP molecules (dark blue) correlated linearly with average FtsZ treadmilling speed, as previously also observed for FtsI (cyan)[11]. **l**. Cumulative distribution function (CDF, open circles) and the corresponding two-population fitting (solid curves) of the moving speed distribution of FtsW-RFP in FtsZ WT and GTPase mutants. The CDF and one-population fitting for FtsZ's treadmilling speed distribution (blue, far right) are shown for comparison. The two-population fitting results were used to plot the fast-moving (red) and slow-moving (green) populations in **j**. **m**. Average speeds of the slow- (green) and fast-moving (red) populations of FtsW-RFP obtained from CDF fitting in **j** *v.s.* FtsZ treadmilling speed in FtsZ GTPase mutant strains[11].

Figure 3: The slow-moving population of FtsW increases with enhanced sPG synthesis activity and depletes with reduced sPG synthesis activity. a. Histograms of directional moving speeds of FtsW^{I302C}-RFP in JXY559 (*ftsW*^{I302C}) in the absence (black) and presence (lime) of MTSES, FtsW-RFP in TB28 (WT, gray), and the superfission variant FtsW^{E289G}-RFP in the same background (strain PM17, *ftsW*^{E289G}, dark green). Note clear shifts to higher speeds in the histogram of FtsW^{I302C}-RFP with MTSES (lime) and to lower speeds in the histogram of FtsW^{E289G}-RFP (dark green) compared to the corresponding WT histograms. Dashed green and red lines marks speeds at 8 nm/s and 29 nm/s respectively for guide of eyes. **b**. CDF (circles) of histograms in **a** and the corresponding best fits (solid curves). Note the left shift of a CDF corresponds to a slower speed with enhanced sPG synthesis activity and the right shift corresponds to a higher speed with reduced sPG synthesis activity. **c**. Histograms of directional moving speeds of FtsW-RFP in BW25113 (wt) without (black) or with aztreonam to inhibit FtsI (purple) and in the superfission variant PM6 (*ftsI*^{R167S}, red). **d.** CDF (circles) of histograms in **c** and the corresponding best fits (solid curves). **e**. Histograms of directional moving speeds of FtsW-RFP in rich defined EZRD medium (yellow) and in Fosfomycin-treated cells (orange). **f**. CDF (circles) of histograms in **e** and the

corresponding best fits (solid curves). **g**. Percentage of time FtsW-RFP and its variants spent in stationary mode correlates inversely with expected sPG synthesis activity.

Figure 4. FtsN plays an important role in promoting the slow-moving population of FtsW. **a**. Bright-field images of WT (TB28), superfission *ftsB*^{E56A} (BL167), *ftsB*^{E56A} Δ*ftsN* (BL173), and FtsN-depleted cells (EC1908). **b**. Histograms of directional moving speeds of FtsW-RFP in superfission variant *ftsB*^{E56A} (orange), WT (grey), *ftsB*^{E56A} Δ*ftsN* (yellow), and FtsN-depleted (blue) cells. **c**. CDF (circles) of histograms in **b** and the corresponding best fits (solid curves).

Figure 5. A two-track model integrating spatial information into the regulation of sPG synthase activity. **a**. Summary plot showing that when sPG synthesis activity is inhibited the average speeds of all directional moving FtsW molecules increases due to the increased fraction of the fast-moving, inactive FtsW population; conversely, when sPG synthesis activity is enhanced, the average speed of FtsW decreases due to the increased fraction of the slow-moving, active FtsW population. **b**. A two-track model depicting that when the synthase FtsWI complex follows the treadmilling FtsZ track it remains inactive but becomes active on the sPG track once it exits the Z-track. FtsN plays an important role in promoting the release of FtsWI from the Z-track to pursue sPG synthesis on the sPG track.

415 **Fig 1**

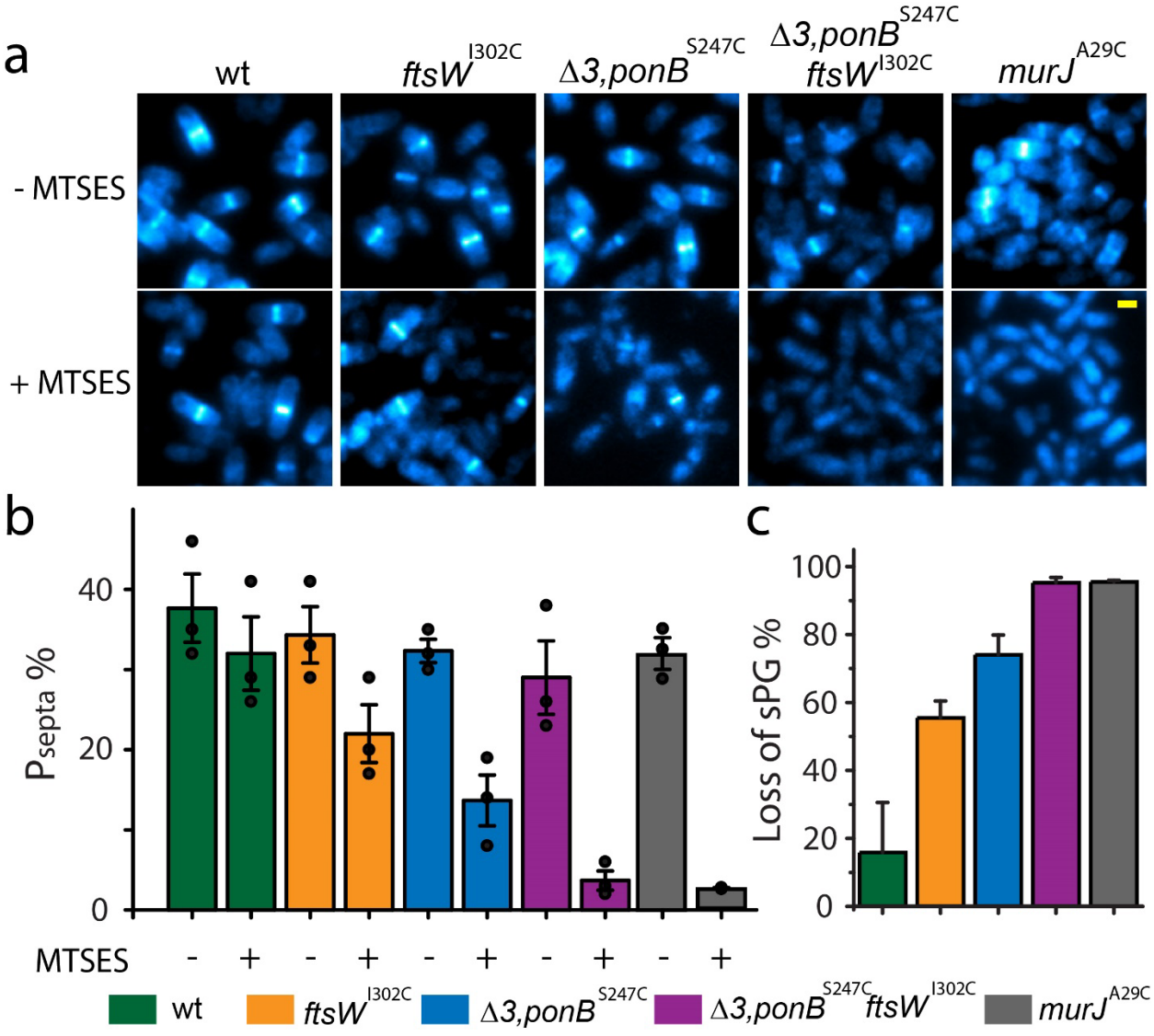

416

417

418 **Fig 2**

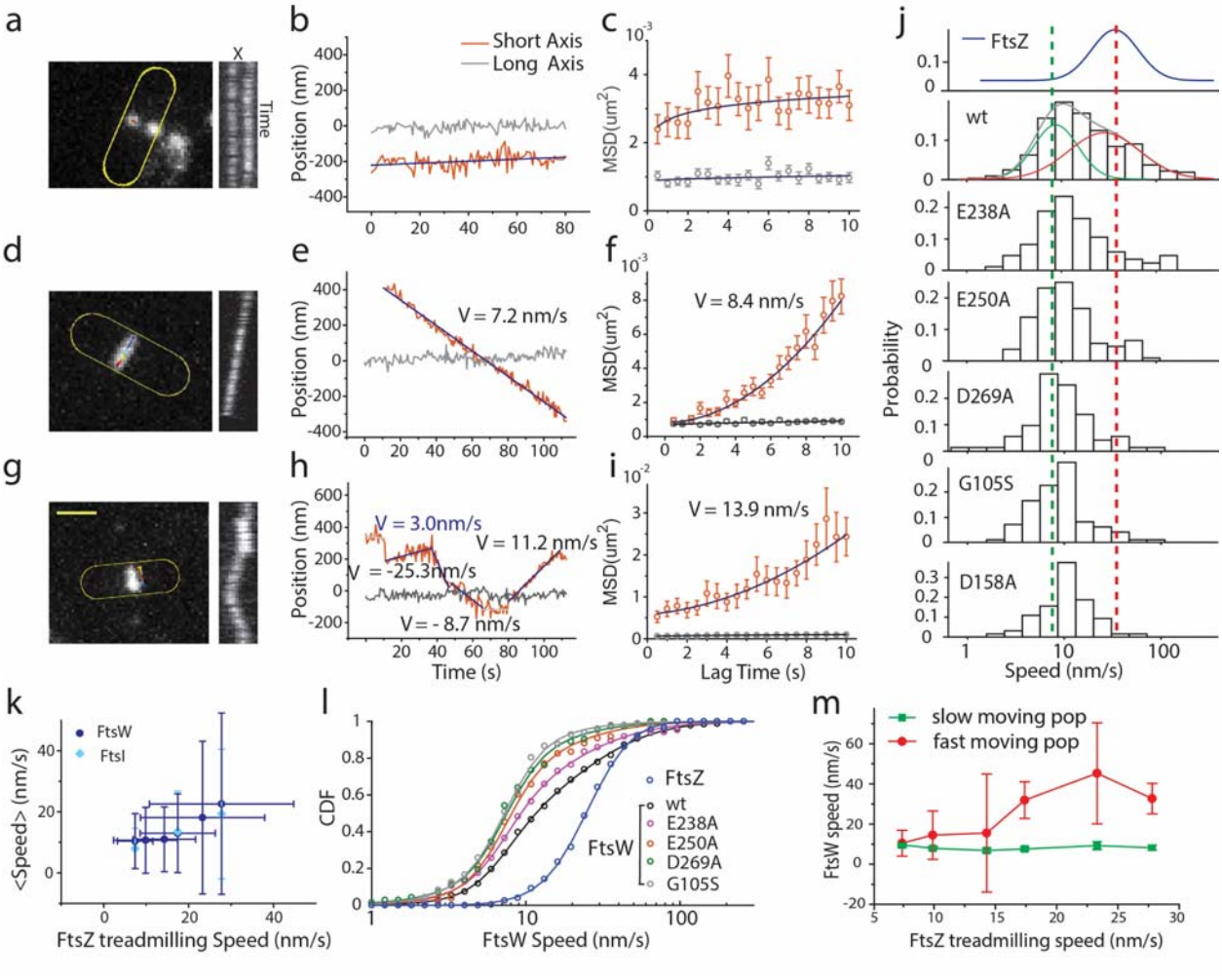

419

Fig 3

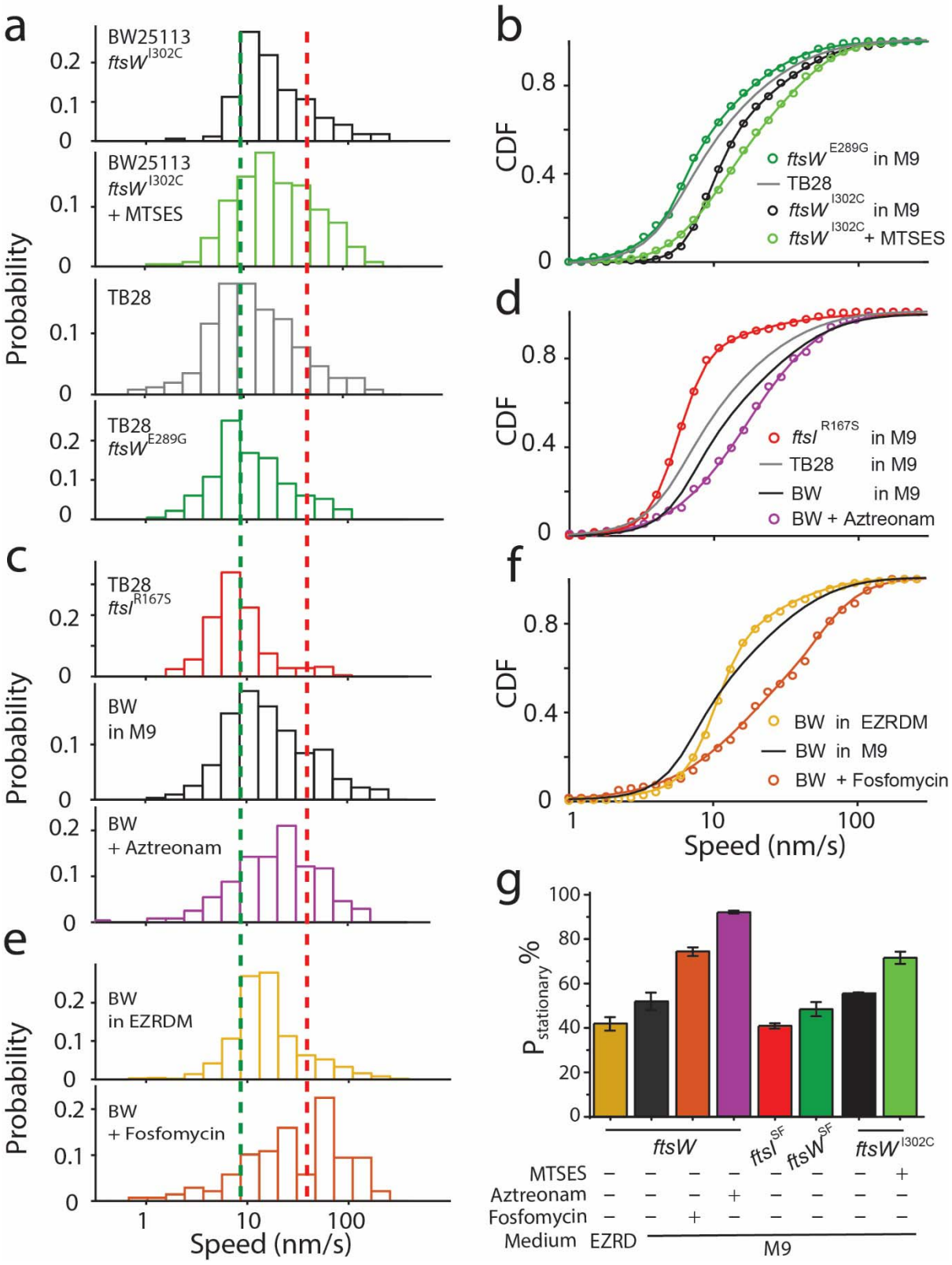

422 **Fig 4**

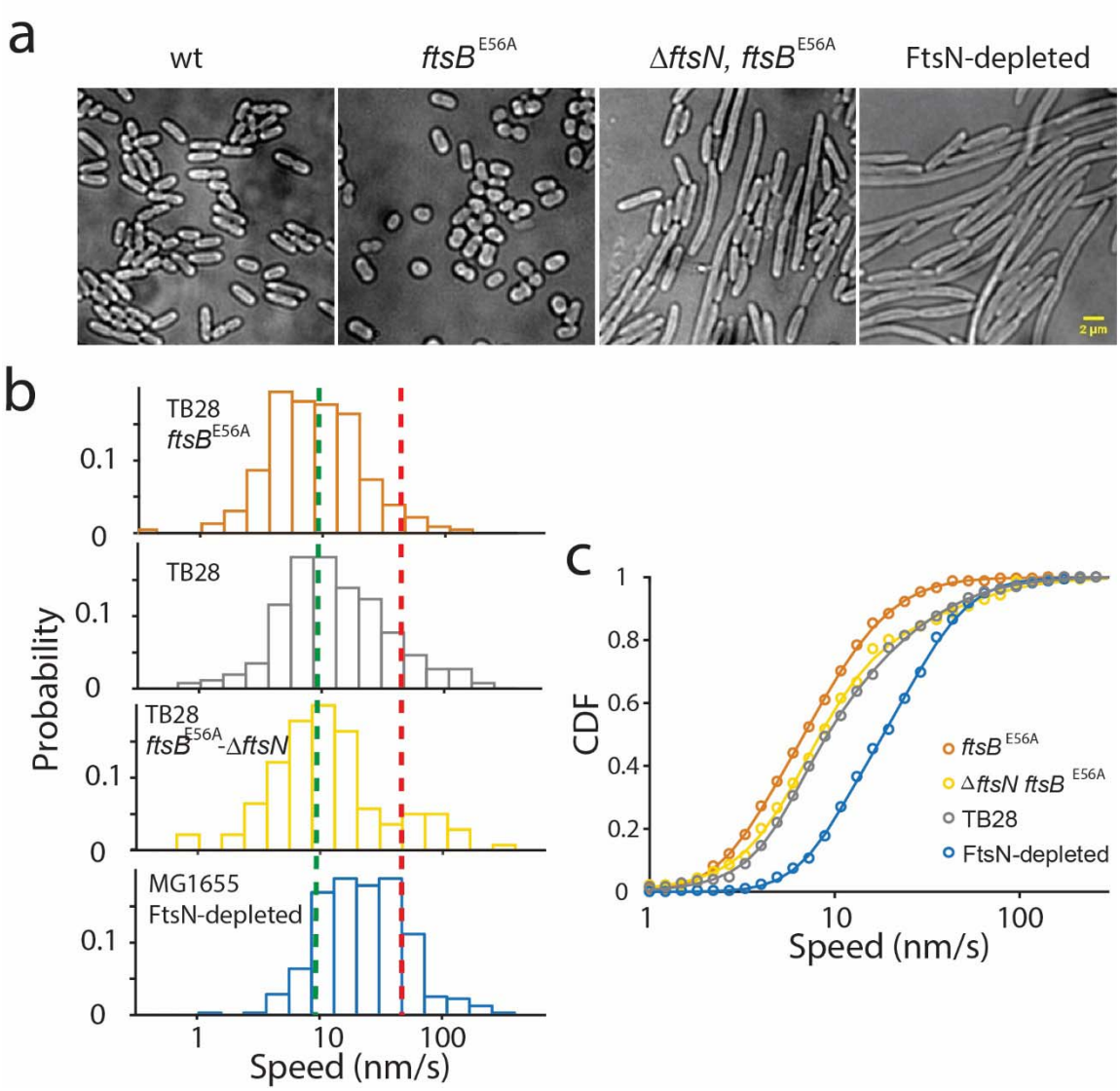

423

424 **Fig 5**

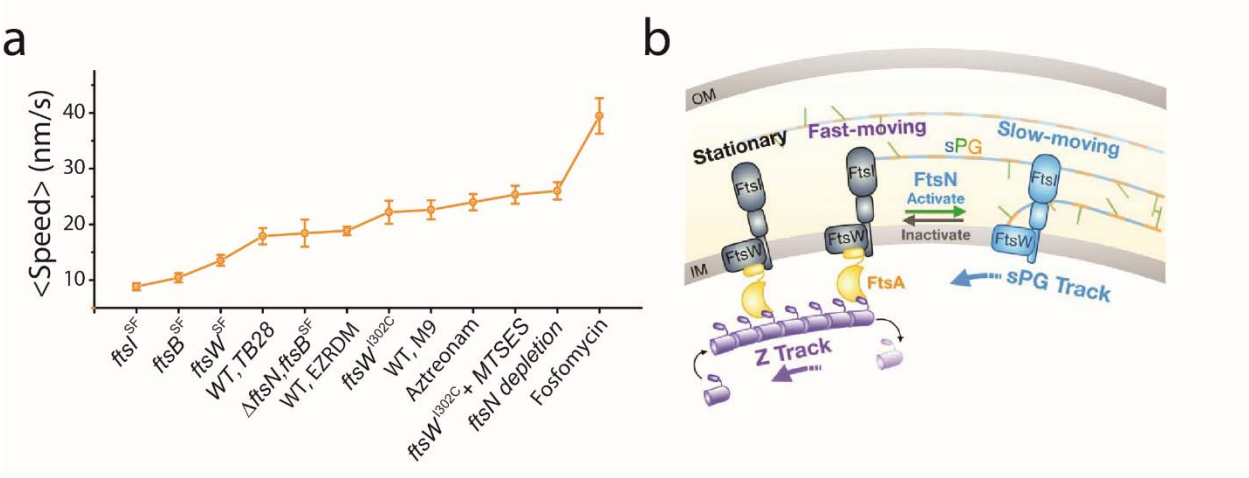

425